Exploring the Essence of Three-Phase Packed Distillation: Substantial Mass Transfer Computation

ARTICLE *in* INDUSTRIAL & ENGINEERING CHEMISTRY RESEARCH · DECEMBER 2009

Impact Factor: 2.59 · DOI: 10.1021/ie9010645

4 AUTHORS, INCLUDING:

Liang Chen
Suzhou University
8 PUBLICATIONS **32** CITATIONS
SEE PROFILE

Jens-Uwe Repke
Technische Universität Bergakademie Frei…
169 PUBLICATIONS **799** CITATIONS
SEE PROFILE

Günter Wozny
Technische Universität Berlin
497 PUBLICATIONS **2,678** CITATIONS
SEE PROFILE

Exploring the Essence of Three-Phase Packed Distillation: Substantial Mass Transfer Computation

Liang Chen,*,† Jens-Uwe Repke,‡ Günter Wozny,‡ and Shuqing Wang§

College of Mechanical-electrical Engineering, Soochow University, 215021, Suzhou, China, Institute of Process Engineering, Technische Universität Berlin, 10623, Berlin, Germany, and State Key Lab of Industrial Control Technology, Zhejiang University, 310027, Hangzhou, China

Three-phase packed distillation has been so far relatively poorly understood. Hence, a substantial mass transfer model describing the (vapor−liquid−liquid) three-phase flow in packed column is proposed to explore the essence of three-phase distillation. The model enables, for the first time, rigorous computation of all the interphase transfer parameters on the basis of a thorough consideration of the unique flow behaviors (such as film breakup, rivulet-flow, surface variation, etc.) caused by the second liquid. The derived theoretical mass transfer model has been incorporated into the three-phase nonequilibrium simulation. Moreover, comprehensive experimental investigations have been carried out using two laboratory-scale columns, and four different packings (Montz-Pak B1-350, Rombopak 9M, Raschig Super-Ring 0.3, and Sulzer Optiflow C.36) were considered. The derived experimental database, covering a wide range of load conditions, is used for flow pattern identification and model validation. For the studied *n*-butanol/water/*n*-propanol system, it is revealed that the flow pattern of the second liquid (aqueous phase) could play a critical role in the system performance. When the second liquid flows below the first liquid film, it will enlarge the interfacial area and enhance the vapor−liquid mass transfer; when the second liquid flows above the first liquid film, it will reduce the interfacial area and degrade the mass transfer. This fundamental flow behavior may essentially result in the discrepancy existing in the highly variable separation efficiencies in three-phase packed columns.

1. Introduction

From a conventional point of view, the presence of more than one liquid phase within a distillation column should be generally avoided because of the uncertainties and troubles introduced by the second liquid. In the past decades, however, heterogeneous azeotropic distillation, where two immiscible liquids appear, has been regarded as one of the most important techniques to break azeotrope and separate close-boiling mixtures. Moreover, vapor−liquid−liquid (three-phase) distillation is frequently encountered in steam-distillation in the petrochemical industry for the recovery and purification of light aromatics such as benzene and toluene.[1] Three-phase distillation can also be used to separate thermally unstable substances.[2] In reactive distillation with liquid−liquid splitting, the unusual vapor−liquid−liquid flow behavior also plays an important role in system performance.[3–5]

Concerning the above three-phase applications, a rigorous and reliable model is of great significance to perform process design, simulation, optimization, and synthesis. However, it is still difficult to derive such a model due to the lack of knowledge on the complexity of vapor−liquid−liquid hydrodynamics. Numerous efforts have been made to improve the model accuracy for three-phase distillation. In an early stage of model development, the equilibrium (EQ) approach was generally adopted for simulation,[6–10] optimization,[11–13] bifurcation (multisteady state) analysis,[14,15] and experimental validation.[16–19] The main weakness of the EQ approach is the use of empirical stage efficiency (tray column) and HETPs (packed column), which are unreliable and unpredictable for multicomponent and multiphase systems.[1,20] Experimental evidence has verified that component efficiencies are not equal to each other and can vary from $-\infty$ to $+\infty$.[21] Cairns and Furzer[19] explicitly warned against incorporating stage efficiency into the simulation for three-phase tray column. In general, the EQ model is regarded as an empirical-based approach. The limitations of this approach may cause great deviations in complex three-phase distillation processes.[20,27]

A new generation of three-phase distillation model using nonequilibrium (NEQ, or rate-based) approach has stepped on the stage since the 1990s.[1] The three-phase NEQ model, dominated by the fundamental mass and heat transfer equations, is certainly more rigorous in nature and superior in theory for tray columns[22–24] and for packed columns.[25–27,58] Compared with the EQ model, the NEQ model avoids the use of empirical stage efficiency and HETPs. The main uncertainty of the NEQ approach is the lack of a reliable mass transfer model to compute the needed set of transfer parameters (e.g., effective interfacial area and mass transfer coefficients, etc.). Concerning three-phase distillation, it is even more difficult because there are three interfaces existing for mass and heat transfer. In tray columns, Lao and Taylor proposed four potential flow models and made some preliminary assumptions (e.g., liquid−liquid equilibrium) to simplify the mass transfer computation.[1] In a continued research, Higler and co-workers improved the so-called "dispersed liquid flow model" and "stratified liquid flow model".[23] Their publication contains detailed computing methods for interfacial areas and vapor-side and liquid-side mass transfer coefficients for tray columns.[23,37] In packed columns, to the best of our knowledge, there were no such methods available for the transfer parameters until now.

This bottleneck limits the application of the NEQ approach, and represents the main obstacle that prevents understanding the intrinsic features of three-phase packed distillation, where discrepant and inconsistent results (separation efficiency) have

* To whom correspondence should be addressed. E-mail: onewheat@live.de.
† Soochow University.
‡ Technische Universität Berlin.
§ Zhejiang University.

10.1021/ie9010645
Published on Web 12/09/2009

Table 1. Experimental Investigations on Separation Efficiency of Three-Phase Packed Distillation

system	packing	results[a]	source
trichloroethylene/toluene/water	Carbon Raschig Rings	↓	Schoenborn[28]
acetone/water/MIBK	Slotted metal Ring	↓	Harrison[29]
n-propanol/*n*-butanol/water	Sulzer Optiflow C.36	↓	Repke[29]
	Montz-Pak B1−350	↑	Villain and Repke[33–35]
	Rombopak 9M	→,↑	
	Raschig Super-Ring 0.3	→,↑	
	Metal Pall Rings	↓	Siegert[32]
ethanol/cyclohexane/water	Sulzer Optiflow C.36	↑	Repke[26]
ethanol/hexane/water	Metal Pall Ring	→	Siegert[31]
acetone/toluene/water	Glass/Ceramic Raschig Rings	↓	Krämer[30]
	Montz-Pak B1−350	↑	Villain and Repke[33–35]
	Rombopak 9M		
	Raschig Super-Ring 0.3		
	Metal Pall Rings	→	Siegert[31,32]
	Sulzer Optiflow C.36	→	Repke[26]
acetone/hexane/water	Glass/Ceramic Raschig Rings	↓	Krämer[30]
hexane/heptane/water	Glass/Ceramic Raschig Rings	→	Krämer[30]
	Metal Pall Rings	↑	Siegert[31]
acetone/methanol/hexane	Ceramic Raschig Rings	↓	Krämer[30]
methanol/toluene/cyclohexane	Raschig Super-Ring 0.3	↓	Villain and Repke[33–35]
	Rombopak 9M		
acetone/tetrachloroethylene/water	Glass/Ceramic Raschig Rings	↓	Krämer[30]
	Raschig Super-Ring 0.3	↑	Villain and Repke[33–35]
	Rombopak 9M		

[a] Compared with two-phase distillation, the separation efficiency of three-phase distillation is ↓ decreased; → unchanged; ↑ increased.

been reported.[26–35] However, the reason for the change of separation efficiency has seldom been successfully explained, because the fluid dynamics and mass transfer mechanism of three-phase distillation are still not well understood.

The earliest experimental investigation on the three-phase packed distillation by Schoenborn et al. (1941) reported a decrease in packing efficiency less than 10%.[28] The authors neglected the decrease and extraordinary fluid dynamic effect. The next publication by Harrison[29] indicated a much larger efficiency decrease of more than 40% in three-phase packed column. The reasons for the decrease were pointed out as the reduction of the interfacial area for mass transfer and liquid maldistribution. Krämer,[30] Siegert et al.,[31,32] Repke et al.,[26] and Villain et al.[33–35] have carried out extensive investigations on three-phase packed distillation. These results are summarized in Table 1, and demonstrate discrepancy and multiplicity even for the same component mixture. Taking the *n*-butanol/water/*n*-propanol system for example, decreased efficiencies in three-phase packed columns were reported by Siegert[32] and Repke et al.[26] However, a later research on *n*-butanol/water/*n*-propanol system by Villain et al.[33–35] reported contrary results, i.e., increased (or unchanged) separation efficiencies were found for most of the experiments they did. The discrepancy in these results made the separation efficiency in a three-phase packed column seem too mysterious to be predicted.

Generally, the occurrence of the second liquid phase will have either negative or positive effects on the separation efficiency. In the literature, however, there is still no deterministic conclusion concerning this point. It is recognized that there are abundant factors (e.g., component mixture, packing geometry, column internals, and operation conditions, etc.) that may affect the performance of three-phase packed columns. The motivation of this research is to develop a theoretical vapor−liquid−liquid mass transfer model applicable for three-phase NEQ simulation, attempting to give a reasonable explanation to the incompatible results on three-phase separation efficiency.

To develop a mass transfer model, research from both the microscopic view (to study vapor−liquid−liquid flow behaviors on packing elements) and the macroscopic view (to collect experimental data using a laboratory-scale packed column) is needed. Recently, a few experimental[38,39,56] and computational fluid dynamics (CFD) studies[40–45] about the flow behaviors on packing surface have been published. As pointed out by Taylor,[36] the work by Repke et al.[43–45] is of particular interest because their simulations show film breakup and rivulet-flow in systems that can have multiple liquid phases. Hence, their observations are used as fundamental assumptions in developing a mass transfer model. Meanwhile, systematic investigations on two-phase and three-phase packed distillations have been carried out at the Institute of Process Engineering, TU Berlin. At this stage, a number of about 200 experiments for *n*-butanol/water/*n*-propanol system carried out using two laboratory-scale columns and four different packings (Montz-Pak B1-350, Rombopak 9M, Raschig Super-Ring 0.3, and Sulzer Optiflow C.36) are considered to identify the three-phase flow pattern, and to validate the three-phase mass transfer model, and further to compare the change of separation efficiencies caused by the appearance of the second liquid. This study may serve as the first attempt toward deriving a reliable mass transfer model for three-phase packed distillation.

2. Theoretical Mass Transfer Model Development

2.1. Prior Works: Investigation on Three-Phase Flow Behavior. A basic understanding of the vapor−liquid−liquid fluid dynamics is prior to develop the mass transfer model. On tracking of the three-phase flow behaviors on packing elements, experimental and CFD investigations were carried out in previous works.[38,39,43–45,56]

In the experiments, an inclined stainless steel plate was used as simplified packing because it is difficult to perform effective measurements on the real packings. The inclined angle could vary between 45° and 60°, which are commonly used corrugation angles of commercial structured packings. The flow behaviors can be observed with a CCD camera. The pictures taken enable the identification of the surface velocities, the film thickness, and the wetted area of the plate.

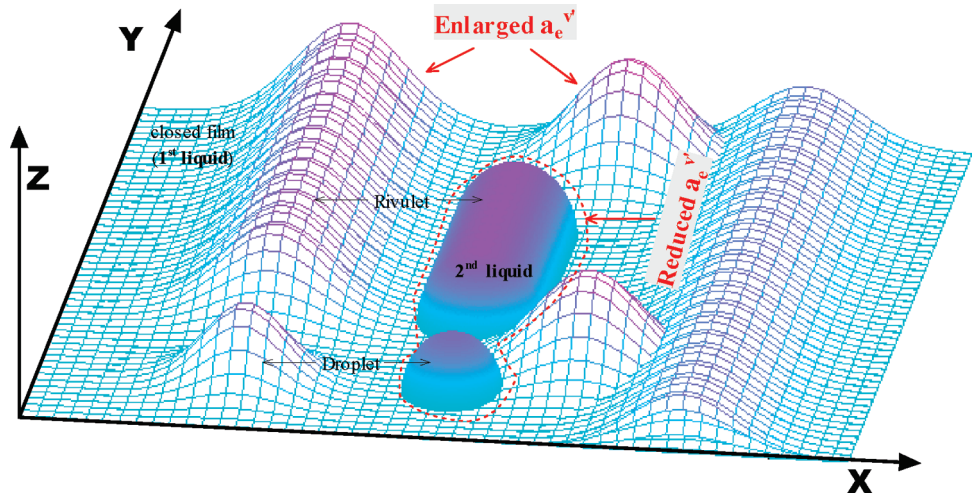

Figure 1. Surface enlargement and reduction on a three-phase packing element.

More details about the experiments can be found in our previous publications.[38,39]

Additionally, CFD investigations were carried out with the commercial software CFX[43,44] and FLUENT.[45] Multiphase liquid-flow described by a complex three-dimensional CFD model was simulated. Flow characteristics such as film breakup and overlaying of different flow patterns were found in good agreement with the experimental results.

Several observations from both experiment-side and simulation-side are summarized as below.

(1) The flow behavior of a two-liquid flow is not just a superposition of the two single-liquid flows.[39] Both liquids interact strongly with each other.

(2) One of the two liquid phases will form a stable closed film (named the first liquid),[38,43–45] while the second liquid will break up and flows as rivulets (and droplets in some cases) even the liquid load higher than the critical point.[39]

(3) Both liquids flow cocurrently and the vapor phase flows count-currently to the liquids.[38,39,43–45,56]

(4) The second liquid can flow either above or below the first liquid film.[38,39,44]

(5) The second liquid flows faster than the first liquid,[39,44,56] i.e., $U_r > U_f$. Here, U_r and U_f represent the superficial velocities for the second liquid rivulets and the first liquid film, respectively.

(6) For the considered system, the second liquid rivulets are thicker than the first liquid film,[44,45] i.e., $\delta_r > \delta_f$. Here, δ_r and δ_f represent the film thicknesses of the rivulets and the film, respectively.

These qualitative conclusions are utilized as fundamental assumptions in developing a quantitative mass transfer model for three-phase packed distillation.

2.2. Essential ideas. The effective interfacial areas are crucial to the interphase mass transfer. Considering three-phase packed distillation, previous research[46,55] has shown that the effective interfacial area $a_e^{V'}$ (between the vapor phase V and the first liquid phase L') is the most dominating transfer parameter. When an immiscible second liquid appears, the effective interfacial area $a_e^{V'}$ will be enlarged or reduced according to different flow patterns of the second liquid. These phenomena are illustrated in Figure 1. If the second liquid flows below the first liquid film (defined as flow pattern 1), an enlargement of $a_e^{V'}$ is observed due to the bulges of the rivulets and droplets. If the second liquid flows above the first liquid film (defined as flow pattern 2), a reduction of $a_e^{V'}$ is expected, because the area covered by the second liquid would be excluded from mass transfer. This flow behavior accounts for the variation of the interfacial area, and could have a substantial effect on the mass transfer performance. The essential idea of this research is to develop a theoretical mass transfer model that takes into account the above features, in order to improve the model accuracy for three-phase NEQ simulation.

To rigorously model a three-phase flow, the following assumptions are made to handle the real conditions.

• The first liquid flows as a flat closed film.

• The second liquid flows mainly as rivulets, the droplets are of small amount and only considered under high load operations, where the rivulets agitated by strong up-flow vapor may split into large amount of droplets.

• The rivulets are of half-cylinder shape; the droplets are of half-ball shape.

• All the rivulets and droplets are supposed to have the same thickness.

During the model development, we introduce two extra hydraulic parameters, which are crucial in analyzing the two-liquid flow system.[26,31,35]

ϕ: Volumetric ratio of the second/first liquid phase, $\phi \in [0,1]$. If $\phi > 1$, phase inversion occurs (i.e., the first liquid will turn into a dispersed liquid phase, and the second liquid will be the continued liquid phase).

η: The proportion of the second liquid flowing below the first liquid film (named as flow pattern parameter in this study), $\eta \in [0,1]$.

Given a three-phase distillation system with a volume flow rate of $\dot{V}_1$ for the first liquid phase, the volume flow rate of the second liquid (rivulets) is $\dot{V}_r = \phi\dot{V}_1$, of which a total amount of $\eta\phi\dot{V}_1$ rivulets flow below the first liquid film.

Unit Surface Enlargement and Reduction. Referring to Figure A1, the unit surface enlargement factor f^+ achieved by a single rivulet is given in Appendix 1.

$$f^+ = \frac{\pi}{2} \quad \text{with} \quad \phi_{\min}^+ = (2\delta_f/\delta_r + (\delta_f/\delta_r)^2)^{-1} \tag{1}$$

and the unit surface reduction factor f^- achieved by a single rivulet is illustrated in Figure A2 in Appendix 1.

$$f^- = 0 \quad \text{with} \quad \phi_{\min}^- = \pi\delta_r/4\delta_f \tag{2}$$

where $\phi_{\min}^+$ (or $\phi_{\min}^-$) is the minimum volumetric ratio of the second/first liquid phase needed to achieve the enlargement (or reduction).

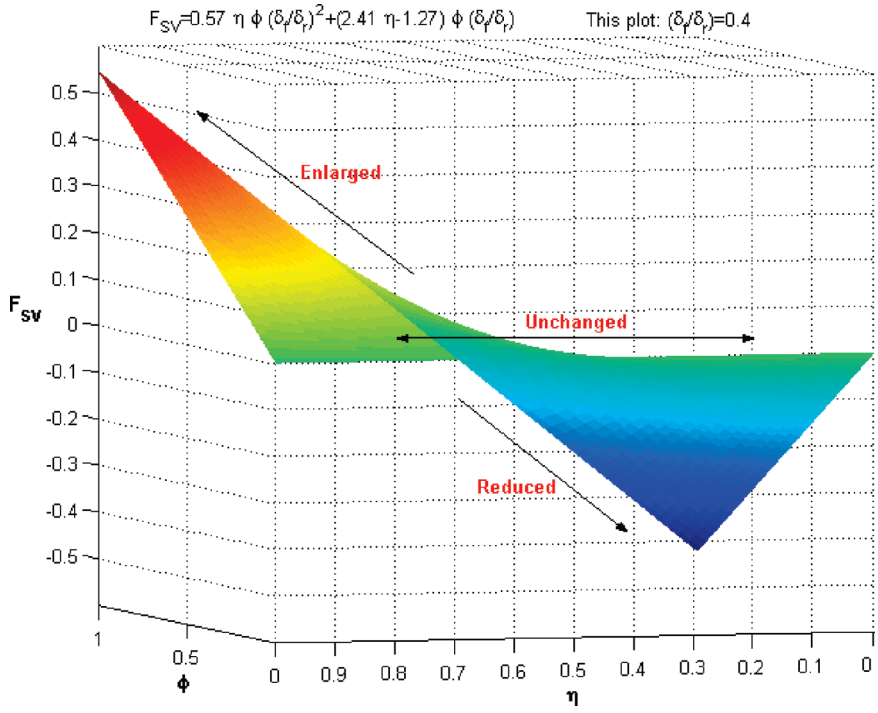

Figure 2. Analysis of the surface variation by a 3-D plot of eq 6.

In the following sections, both cases of surface enlargement and surface reduction are deduced.

Surface Enlargement. Supposing that all the second liquid rivulets flow as pattern 1 (i.e., below the first liquid film), the effect of surface enlargement can be expressed by the enlargement factor F^+ and calculated as

$$F^+ = \frac{\dot{V}_r}{\dot{V}_1\phi^+_{\min}}(f^+ - 1) = \left(\frac{\pi}{2} - 1\right)\phi\left(2\frac{\delta_f}{\delta_r} + \left(\frac{\delta_f}{\delta_r}\right)^2\right) \quad (3)$$

Surface Reduction. Supposing that all the second liquid rivulets flow as pattern 2 (i.e., above the first liquid film), the effect of surface reduction can be expressed by the reduction factor F^-

$$F^- = \frac{\dot{V}_r}{\dot{V}_1\phi^-_{\min}}(f^- - 1) = -\phi\frac{4\delta_f}{\pi\delta_r} \quad (4)$$

Overall Surface Variation. In fact, the second liquid may flow partly below and partly above the first liquid film (i.e., a mixed flow of pattern 1 and pattern 2).

To match the real conditions, the flow pattern parameter η defined above is introduced to calculate the overall surface variation factor F_{SV}.

$$F_{SV} = \eta F^+ + (1 - \eta)F^- \quad (5)$$

Substituting eqs 3 and 4 into eq 5, we derive

$$F_{SV} = \left(\frac{\pi}{2} - 1\right)\eta\phi\left(2\frac{\delta_f}{\delta_r} + \left(\frac{\delta_f}{\delta_r}\right)^2\right) + \frac{4}{\pi}(\eta - 1)\phi\frac{\delta_f}{\delta_r}$$
$$\approx 0.57\eta\phi\left(\frac{\delta_f}{\delta_r}\right)^2 + (2.41\eta - 1.27)\phi\frac{\delta_f}{\delta_r} \quad (6)$$

$F_{SV} \in [-1, 1]$. To give a virtual illustration of eq 6, a graphical analysis with 3-D plot is shown in Figure 2. There are three (i.e., reduced, unchanged, enlarged) regions concerning surface variation of a_e^V. Remarks are given below.

(1) If there is no second liquid, the surface area is unchanged (i.e., $\phi \to 0$, $F_{SV} \to 0$).
(2) When the second liquid flows mainly as pattern 2 (i.e., $\eta \in [0.0,0.4]$), the surface reduction is achieved. Referring to eq 4, the surface area will linearly decrease as the second liquid appears more and more.
(3) When the second liquid flows mainly as pattern 1 (i.e., $\eta \in [0.6,1.0]$), the surface enlargement is achieved. Referring to eq 3, the surface area will linearly increase as the second liquid appears more and more.
(4) When $\phi \to \phi^+_{\min}$ and $\eta = 1$, $F_{SV} \to (f^+ - 1) = (\pi/2 - 1) \approx 0.57$, i.e. when sufficient amount of the second liquid rivulets flow below and lift the first liquid film, the maximum surface enlargement is $\pi/2$.

3. Incorporating Mass Transfer Computation into NEQ Approach

3.1. Rate-Based Mass Transfer. For multicomponent and multiphase distillations, the NEQ or rate-based approach has evolved as the most dominating way of modeling to avoid entirely a prior knowledge of component-specific efficiency and HETPs.[36]

Below, the rate-based mass transfer computation for three-phase packed distillation is developed on the basis of model assumptions by Krishnamurthy and Taylor,[47] and Repke et al.[24]

The key concept of the rate-based approach is the direct calculation of the interphase mass transfer, which is frequently described as[21]

$$N_i \cdot a = \left(J_i + z_i\sum_{i=1}^{N_C} N_i\right)\cdot a \quad (7)$$

where N_i is the molar flux of component i, and a is the interfacial area. Considering a three-phase packing segment illustrated in Figure 3, there are three interfaces and six molar fluxes existing for mass transfer, i.e.,

$$N_i^{V'} \cdot a^{V'} = \left(J_i^{V'} + y_i \sum_{i=1}^{N_C} N_i^{V'}\right) \cdot a^{V'} = N_i'^{V} \cdot a^{V'} = \left(J_i'^{V} + x_i' \sum_{i=1}^{N_C} N_i'^{V}\right) \cdot a^{V'} \quad (8)$$

$$N_i^{V''} \cdot a^{V''} = \left(J_i^{V''} + y_i \sum_{i=1}^{N_C} N_i^{V''}\right) \cdot a^{V''} = N_i''^{V} \cdot a^{V''} = \left(J_i''^{V} + x_i'' \sum_{i=1}^{N_C} N_i''^{V}\right) \cdot a^{V''} \quad (9)$$

$$N_i'^{-''} \cdot a'^{-''} = \left(J_i'^{-''} + x_i' \sum_{i=1}^{N_C} N_i'^{-''}\right) \cdot a'^{-''} = N_i''^{-'} \cdot a'^{-''} = \left(J_i''^{-'} + x_i'' \sum_{i=1}^{N_C} N_i''^{-'}\right) \cdot a'^{-''} \quad (10)$$

where J_i is the molar diffusion flux of component i, and it can be calculated as

$$\mathbf{J}^{V'} = c_t^{V}[\mathbf{k}^{V'}](\mathbf{y} - \mathbf{y}^{V'}), \quad \mathbf{J}'^{V} = c_t'[\mathbf{k}'^{V}](\mathbf{x}'^{V} - \mathbf{x}') \quad (11)$$

$$\mathbf{J}^{V''} = c_t^{V}[\mathbf{k}^{V''}](\mathbf{y} - \mathbf{y}^{V''}), \quad \mathbf{J}''^{V} = c_t''[\mathbf{k}''^{V}](\mathbf{x}''^{V} - \mathbf{x}'') \quad (12)$$

$$\mathbf{J}'^{-''} = c_t'[\mathbf{k}'^{-''}](\mathbf{x}'^{-''} - \mathbf{x}'), \quad \mathbf{J}''^{-'} = c_t''[\mathbf{k}''^{-'}](\mathbf{x}''^{-'} - \mathbf{x}'') \quad (13)$$

where $[\mathbf{k}]$ is the matrix of multicomponent mass transfer coefficients with order $n - 1$. There are some methods to calculate the $[\mathbf{k}]$ matrix.[21,47,48] The method of Krishna and Standart[48] in which $[\mathbf{k}]$ is related to the binary mass transfer coefficients β through a solution of Maxwell−Stefan equations is adopted in this work, i.e.,

$$[\mathbf{k}] = [\mathbf{B}]^{-1}[\mathbf{\Gamma}][\mathbf{\Xi}] \quad (14)$$

where the matrix $[\mathbf{\Xi}]$ accounts for the influence of the high flux correction factor,[21] and the thermodynamic factor matrix $[\mathbf{\Gamma}]$ can be derived from an activity coefficient model (e.g., NRTL, UNIQUAC, etc.).[21] The matrix $[\mathbf{B}]$ in eq 14 has the elements given by (concerning three-phase distillation)

$$B_{ii}^{V'} = \frac{y_i}{\beta_{in}^{V'}} + \sum_{\substack{k=1 \\ i \neq k}}^{N_C} \frac{y_k}{\beta_{ik}^{V'}}, \quad B_{ij}^{V'} = -y_i\left(\frac{1}{\beta_{ij}^{V'}} - \frac{1}{\beta_{in}^{V'}}\right) \quad (15)$$

$$B_{ii}^{V''} = \frac{y_i}{\beta_{in}^{V''}} + \sum_{\substack{k=1 \\ i \neq k}}^{N_C} \frac{y_k}{\beta_{ik}^{V''}}, \quad B_{ij}^{V''} = -y_i\left(\frac{1}{\beta_{ij}^{V''}} - \frac{1}{\beta_{in}^{V''}}\right) \quad (16)$$

$$B_{ii}'^{V} = \frac{x_i'}{\beta_{in}'^{V}} + \sum_{\substack{k=1 \\ i \neq k}}^{N_C} \frac{x_k'}{\beta_{ik}'^{V}}, \quad B_{ij}'^{V} = -x_i'\left(\frac{1}{\beta_{ij}'^{V}} - \frac{1}{\beta_{in}'^{V}}\right) \quad (17)$$

$$B_{ii}''^{V} = \frac{x_i''}{\beta_{in}''^{V}} + \sum_{\substack{k=1 \\ i \neq k}}^{N_C} \frac{x_k''}{\beta_{ik}''^{V}}, \quad B_{ij}''^{V} = -x_i''\left(\frac{1}{\beta_{ij}''^{V}} - \frac{1}{\beta_{in}''^{V}}\right) \quad (18)$$

$$B_{ii}'^{-''} = \frac{x_i'}{\beta_{in}'^{-''}} + \sum_{\substack{k=1 \\ i \neq k}}^{N_C} \frac{x_k'}{\beta_{ik}'^{-''}}, \quad B_{ij}'^{-''} = -x_i'\left(\frac{1}{\beta_{ij}'^{-''}} - \frac{1}{\beta_{in}'^{-''}}\right) \quad (19)$$

$$B_{ii}''^{-'} = \frac{x_i''}{\beta_{in}''^{-'}} + \sum_{\substack{k=1 \\ i \neq k}}^{N_C} \frac{x_k''}{\beta_{ik}''^{-'}}, \quad B_{ij}''^{-'} = -x_i''\left(\frac{1}{\beta_{ij}''^{-'}} - \frac{1}{\beta_{in}''^{-'}}\right) \quad (20)$$

To perform the above mass transfer computation successfully, a prior knowledge of transfer parameters ($a^{V'}$, $a^{V''}$, $a'^{-''}$, $\beta^{V'}$, $\beta^{V''}$, β'^{V}, β''^{V}, $\beta'^{-''}$, $\beta''^{-'}$) is needed. These parameters (or correlations to predict these parameters), however, are not available in literature. When modeling three-phase distillation, simplifications have been adopted. A liquid−liquid equilibrium,[1,22,24,25,37,46] is assumed to avoid using parameters ($a'^{-''}$, $\beta'^{-''}$, $\beta''^{-'}$). Some publications[24,46] made further assumptions to ignore the interaction between vapor phase and the second liquid phase to avoid parameters ($a^{V''}$, $\beta^{V''}$, β''^{V}).

This paper considers the mass transfers between all V−L′, V−L″, L′−L″ interfaces, i.e. the transfer parameters ($a^{V'}$, $a^{V''}$, $a'^{-''}$, $\beta^{V'}$, $\beta^{V''}$, β'^{V}, β''^{V}, $\beta'^{-''}$, $\beta''^{-'}$) are all involved in the simulation. Due to the limited space, other NEQ model equations are not presented here, for a reference see 27 and 55. The sensitivity analysis of all the transfer parameter was also given in ref 55. The most sensitive parameter was found to be the interfacial area $a^{V'}$. Its important role to the distillation performance was outlined,[55] which is the direct driving force of this research.

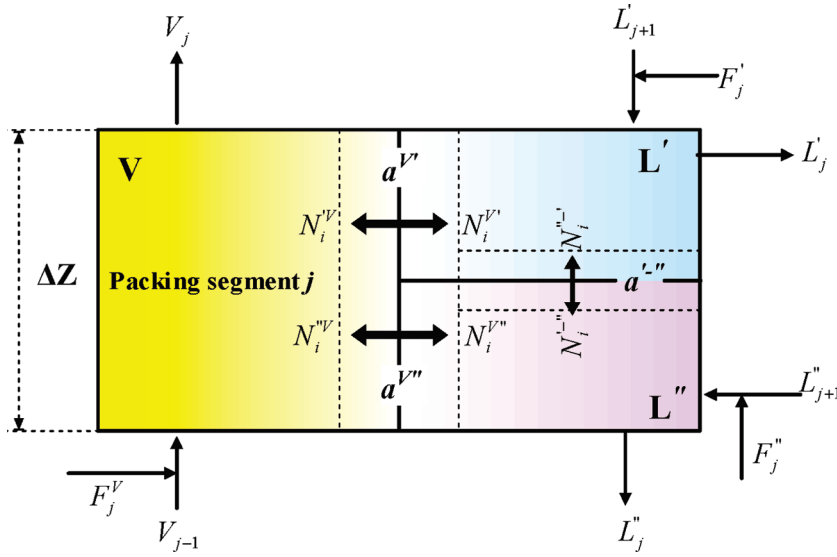

Figure 3. Interphase mass transfer for a three-phase packing segment based on double-film model.

In the following section, the methods to calculate the transfer parameters are presented.

3.2. Three-Phase Mass Transfer Model. Effective Interfacial Area. In the three-phase mass transfer computation, effective interfacial areas ($a_e^{V'}$,$a_e^{V''}$,$a_e^{'-''}$) for all three interfaces are needed. When we consider the effect of surface variation caused by the second liquid, the effective interfacial area $a_e^{V'}$ at the V−L′ interface can be derived as follows.

$$a_e^{V'} = (1 + F_{SV})a_e = \left(1 + (2.41\eta - 1.27)\phi\frac{\delta_f}{\delta_r} + 0.57\eta\phi\left(\frac{\delta_f}{\delta_r}\right)^2\right)\cdot a_e \quad (21)$$

where F_{SV} is the overall surface variation factor derived in eq 6, and a_e is the original vapor−liquid effective interfacial area assuming the second liquid does not appear. It can be calculated with literature correlations[54] for two phase distillation. In this study, a_e is calculated by correlation equations (A9 and A10), which are parts of a two-phase mass transfer model given in Appendix 2. The mass transfer model, containing detailed methods to calculate a_e, β^V, and β^L is validated by two-phase distillation experiments. More details are given in Appendix 2.

To consider column-specified interfacial area $a^{V'}$, the cross section of the column A_c and the height of packing segment ΔZ are needed.

$$a^{V'} = a_e^{V'}\cdot a_p\cdot A_c\cdot\Delta Z \quad (22)$$

One advantage of the proposed mass transfer model is that it can also calculate the effective interfacial areas $a_e^{V''}$,$a_e^{'-''}$ at V−L″ and L′−L″ interfaces. For V−L″ interface, only $(1 - \eta)$ percentage of the second liquid flowing above the first liquid film is related with V−L″ mass transfer. Therefore,

$$a_e^{V''} = \left((1 - \eta)\frac{\dot{V}_r}{\dot{V}_1\phi_{\min}^-}f^+\right)a_e = 2(1 - \eta)\phi\frac{\delta_f}{\delta_r}\cdot a_e \quad (23)$$

$$a^{V''} = a_e^{V''}\cdot a_p\cdot A_c\cdot\Delta Z \quad (24)$$

For L′−L″ interface, the effective interfacial area $a_e^{V''}$ is the summation of the areas related with liquid−liquid contact. Referring to Figures A1 and A2, it can be calculated as

$$a_e^{'-''} = \left(\eta\frac{\dot{V}_r}{\dot{V}_1\phi_{\min}^+}f^+ + (1 - \eta)\frac{\dot{V}_r}{\dot{V}_1\phi_{\min}^-}\cdot 1\right)a_e = \left(1.57\eta\phi\left(\frac{\delta_f}{\delta_r}\right)^2 + (1.27 + 1.87\eta)\phi\frac{\delta_f}{\delta_r}\right)\cdot a_e \quad (25)$$

$$a^{'-''} = a_e^{'-''}\cdot a_p\cdot A_c\cdot\Delta Z \quad (26)$$

It is notable that the proposed method in eqs 21−26 may be the first attempt for computation of the effective interfacial areas $a_e^{V'}$, $a_e^{V''}$, and $a_e^{'-''}$ in a three-phase packed column.

Binary Mass Transfer Coefficients. So far, there is no clear evidence reported that the second liquid will change the mass transfer coefficients. Therefore, at V−L′ interface, we assume that the binary mass transfer coefficients $\beta^{V'}$ and $\beta^{'V}$ can be calculated the same as β^V and β^L by eqs A7 and A8 in Appendix 2.

$$\beta^{V'} = 0.12\frac{D_V}{d_h}(Re_V)^{2/3}(Sc_V)^{1/3} \quad (27)$$

$$\beta^{'V} = 2\sqrt{\frac{D_L'}{\pi t_{res}}} = 2\sqrt{\frac{D_L'U_{Le}'}{\pi d_h}} \quad (28)$$

Table 2. Comparison of the Values for Film Thickness (mm): Experimental Measurement, CFD Simulation, and Correlation Prediction

method	rivulet	film
exp measurement[56]	0.5−1.5	0−0.2
CFD simulation[44]	0.5−1.25	0−0.3
Nicolaiewsky	0.5−1.2	0.1−0.3

For the binary mass transfer coefficients $\beta^{V''}$ at V−L″ interface, previous research[55] has revealed that the aqueous second liquid phase trends to inhibit the mass transfer from vapor phase to the second liquid phase. Therefore, a calibrated coefficient C_β is added to eq 27. The value C_β is adopted from previous research.[55]

$$\beta^{V''} = C_\beta\cdot 0.12\frac{D_V}{d_h}(Re_V)^{2/3}(Sc_V)^{1/3}, \quad C_\beta \in [0.5,\ 0.7] \quad (29)$$

For the liquid-side binary mass transfer coefficients $\beta^{''V}$, the residence time t_{res} in eq 28 is replaced by the formation time t_{form} to consider the formation of the rivulets and droplets.[49]

$$\beta^{''V} = 2\sqrt{\frac{D_L''}{\pi\cdot t_{form}}},\ t_{form} \approx 1.5\text{s} \quad (30)$$

At the L′−L″ interface, the film theory is applied to calculate the binary mass transfer coefficients $\beta^{'-''}$ and $\beta^{''-'}$.[27] Existing experimental data[49] confirm that it is more suitable to calculate the liquid−liquid mass transfer coefficients by film model rather than the penetration model.[21]

$$\beta^{'-''} = \frac{D_L'}{\delta_f} \quad (31)$$

$$\beta^{''-'} = \frac{D_L''}{\delta_r} \quad (32)$$

Hydraulic Parameters. The hydraulic parameters such as film thicknesses, superficial velocities, and liquid holdups are needed in the computation of the effective interfacial areas and binary mass transfer coefficients in eqs 21−32.

In this study, the film thickness is calculated by the Nicolaiewsky correlation[52] given in eq 33, because it is one of the limited publications that consider rivulet-flow.

$$\delta = 2.85\left(\frac{\rho_L^3(g\cos\theta)^2}{\mu_L^2\sigma_L}\right)^{-0.2}(1 - \cos\gamma)^{0.24} \quad (33)$$

The applicability of the Nicolaiewsky correlation is validated by our experiments and CFD simulations.[44] The film thicknesses for film-flow and rivulet-flow predicted by the Nicolaiewsky correlation are given in Table 2. The prediction by Nicolaiewsky correlation is acceptable, and shows good accordance to the experimental and CFD results.

The effective superficial velocities are another set of important hydraulic parameters. They are required in eq A10 to calculate the effective interfacial areas and binary mass transfer coefficients. The definitions were originally introduced by Rocha et al.[57] as below.

$$U_{Le}' = \frac{U_L'}{\varepsilon h_L'\sin\theta} \quad (34)$$

$$U_{Le}'' = \frac{U_L''}{\varepsilon h_L''\sin\theta} \quad (35)$$

$$U_{Ve} = \frac{U_V}{\varepsilon(1 - h_L' - h_L'')\sin\theta} \tag{36}$$

The liquid holdup h_L' needed in the above equations is calculated using Billet and Schultes correlation.[53]

$$h_L' = \left(12\frac{1}{g}\frac{\mu_L}{\rho_L}U_L a_P^{\,2}\right)^{1/3} \tag{37}$$

The holdup of the second liquid can be calculated by eq 38.

$$h_L'' = c_h \phi h_L', \quad (c_h = 0.69) \tag{38}$$

The best fit value for coefficient c_h was found ($c_h = 0.69$), and illustrated briefly below in eqs 39−41.

The superficial velocities of both liquids can be calculated as

$$u_L' = \frac{L'M'}{\rho' A_c}, \quad u_L'' = \frac{L''M''}{\rho'' A_c} \tag{39}$$

and

$$\phi = \frac{L''M''}{\rho''} \Big/ \frac{L'M'}{\rho'} = \frac{u_L''}{u_L'} \tag{40}$$

According to the definition of effective superficial velocities given in eqs 34−36, we can derive

$$\frac{u_{Le}'}{u_{Le}''} = \frac{u_L' h_L''}{u_L'' h_L'} = \phi^{-1}\frac{h_L''}{h_L'} = c_h \tag{41}$$

It is revealed that the second liquid flows faster than the first liquid in a three-phase flow. The ratio measured in previous experiment[56] is about 0.69, i.e., the best fit value is $c_h = 0.69$.

4. Results and Discussion

Experimental investigations have been performed. The derived data sets are used in the following model validation as well as flow pattern identification.

4.1. Experiments. Two laboratory-scale pilot packed columns were built up for experimental investigations at the Institute of Process Engineering, TU Berlin. Both columns are operated under total reflux operation, the F-factor (defined as $U_V\rho_V^{0.5}$) was used as an indicator of the internal state of fluid dynamics and to characterize the operation conditions. The experimental runs covered a wide range of operation conditions (F-factor: 0.2−2.8 $\text{Pa}^{0.5}$).

The studied component mixture was *n*-butanol/water/*n*-propanol. The system has two binary azeotropes (one homogeneous, one heterogeneous), and a limited miscibility gap. In the case of phase splitting, the light component *n*-propanol is dissolved in both existing liquid phases. Therefore, it is regarded as the key component in the following discussions. More information about column configurations and experimental conditions is summarized in Table 3 and described in detail below.

Pilot Plant 1: Low Load Operation. The first experimental investigations were performed at relatively low load (F-factor, 0.2−0.6 $\text{Pa}^{0.5}$) conditions in a 0.07 m diameter column packed with Sulzer Optiflow C.36. Figure 4 shows the process diagram of the pilot plant 1. The column was equipped with 5 packing sections and had an effective packing height of nearly 2.5 m. The liquid and vapor samples were withdrawn along the column. The vapor concentrations are regarded more reliable and used as validation data sets in the study.

Table 3. Column Configuration and Experimental Conditions

	plant 1	plant 2
mixture	*n*-butanol/water/*n*-propanol	
column	total condenser, total reflux, pressure (1 atm)	
	7.5 m height	6.2 m height
	0.07 m diameter	0.1 m diameter
packing	packing sections: 5	packing sections: 1
		Rombopak 9M (0.52 m)
	Sulzer Optiflow C.36 (0.5 m)	Montz-Pak B1−350 (0.6 m)
		Raschig Super-ring 0.3 (0.6 m)
experiments	two-phase runs: 32	two-phase runs: 48
	two-/three-phase runs: 30	three-phase runs: 102
F-factor	0.2−0.6 $\text{Pa}^{0.5}$	0.6−2.8 $\text{Pa}^{0.5}$

According to different feed concentrations, two-phase (vapor−liquid) and three-phase (vapor−liquid−liquid) conditions may appear on certain packing sections. Overall, 32 pure two-phase distillation experiments were carried out, and another 30 mixed two-/three-phase experiments (where two-phase distillation only occurs on the top packing section) were performed. The prior of the liquid phase stability on each packing section was specified in the simulation of the corresponding experiments.

Pilot Plant 2: High Load Operation. As supplementary, more experimental investigations at relatively high load condition (F-factor, 0.6−2.8 $\text{Pa}^{0.5}$) were carried out using another pilot column (see Figure 5). The column has an inner diameter of 0.1 m. It is possible to install four packing sections to a total packing height of 2.4 m. In this study, only one packing section was used (see Figure 5) to carry out experiments of pure two-phase distillation and pure three-phase distillation. The experimental database consists of 48 two-phase distillation runs and 102 three-phase distillation runs. Three kinds of packings (open structured packing, Rombopak 9M; closed structured packing, Montz-Pak B1-350; and random packing, Raschig Super-ring 0.3) were considered for different three-phase hydrodynamics. The samples below and above the packing section are of great importance, since they directly reflect the mass transfer performance. The vapor concentrations are used as the basic data sets for model validation and flow pattern identification described in the following sections.

4.2. Flow Pattern Identification. In the previous sections, a theoretical three-phase mass transfer model was proposed. Rigorous computations are given in eqs 21−38 for most of the transfer parameters except the "flow pattern parameter" η. Until now, neither literature data nor experimental measurement is available to correlate this parameter. Therefore, empirical parameter estimation is employed in this section to identify the flow pattern based on the experimental database derived.

The parameter estimation is carried out in gPROMS. The two-/three-phase NEQ model for packed columns is built up. To successfully solve the simulation, good guess values for model variables are needed. First of all, the number of liquid phases on each packing segment should be given. This is known as a prior determined in the experiments. Then for the given phase distribution, an EQ simulation is carried out. The derived solution is applied to calculate the guess values for all the transfer parameters using the proposed mass transfer model. The guess values for the mass transfer fluxes are computed on the basis of vapor and liquid flow rates and concentration derived in EQ simulation. The guess values for temperatures can be assumed the same as EQ-simulated results.

The simulated predictions $\tilde{\mathbf{y}}$ are compared with the experimental results $\mathbf{y}$, and the flow pattern parameter η can be

estimated using a maximum likelihood objective function $\mathbf{\Phi}$ as given by eq 42.

$$\mathbf{\Phi}(\eta) = \frac{N_P \cdot N_C}{2}\ln(2\pi) + \frac{1}{2}\min_{\eta}\left(\sum_{i=1}^{N_P}\sum_{j=1}^{N_C}\left(\ln(\sigma_{i,j}^2) + \frac{(y_{i,j} - \tilde{y}_{i,j})^2}{\sigma_{i,j}^2}\right)\right)$$

s.t

$$\begin{aligned} &\mathbf{g}(\mathbf{x_i}, \mathbf{y_i}, \mathbf{u}, \eta) = \mathbf{0} \\ &\mathbf{h}(\mathbf{x_i}, \mathbf{y_i}, \mathbf{u}, \eta) \geq \mathbf{0} \\ &i = 1, \cdots, N_P \quad 0 \leq \eta \leq 1 \end{aligned} \tag{42}$$

where $\sigma_{i,j}$ is the variance of the measurement error in $y_{i,j}$.

For each experimental data set, the vapor molar fractions $\mathbf{y}$ contain the measurements on N_P packing sections for N_C components, i.e.,

$$\mathbf{y_i} = [y_{i,1}, y_{i,2}, \cdots, y_{i,N_C}]^T \quad i = 1, \cdots, N_P \tag{43}$$

They are called output variables in the estimation. There are also many unmeasurable state variables $\mathbf{x_i}$ (like effective interfacial areas, liquid holdups, etc.) in the NEQ model equations $\mathbf{g}$ and inequality constrains $\mathbf{h}$.

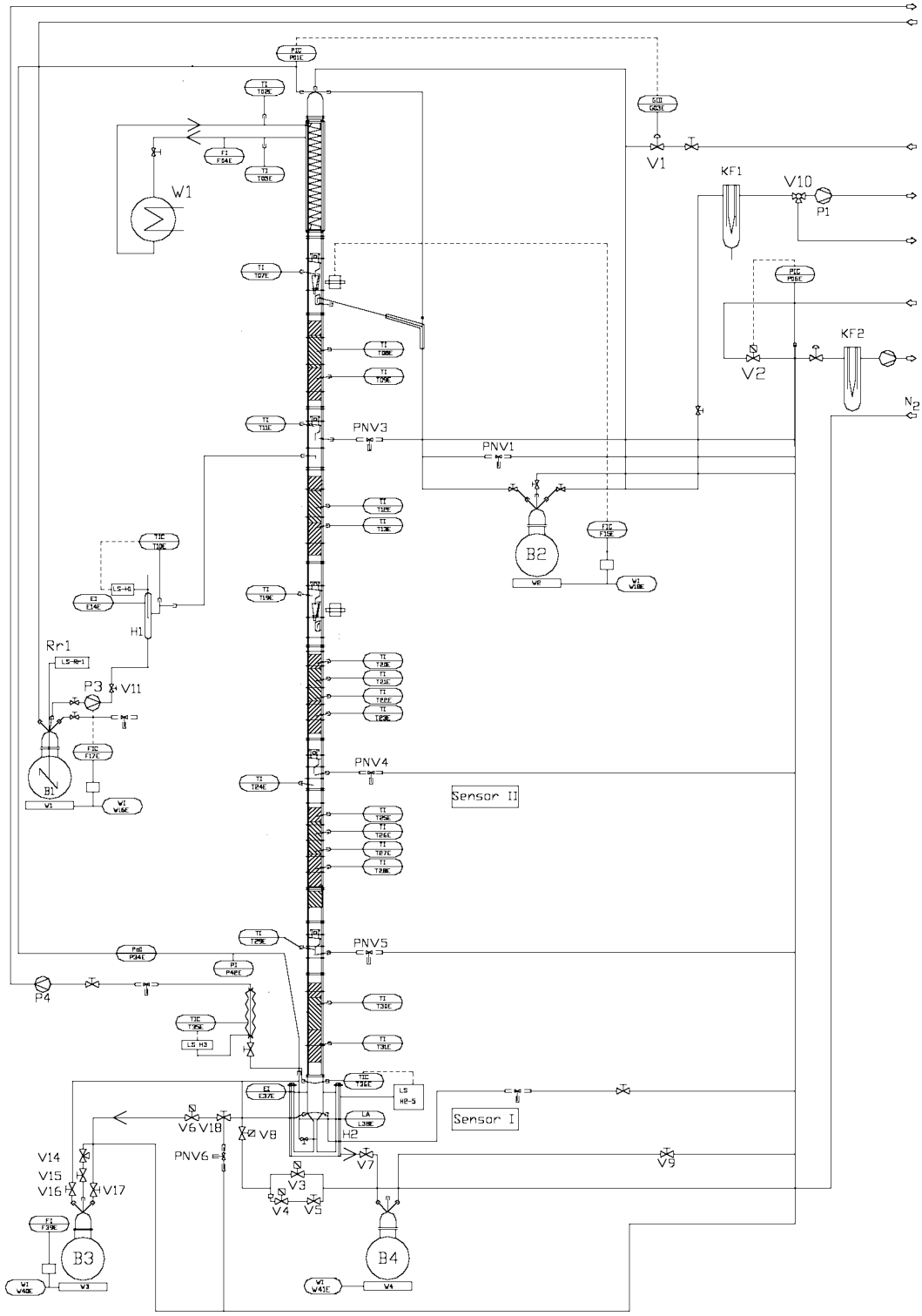

Figure 4. Process diagram of pilot plant 1 (low load conditions).[26]

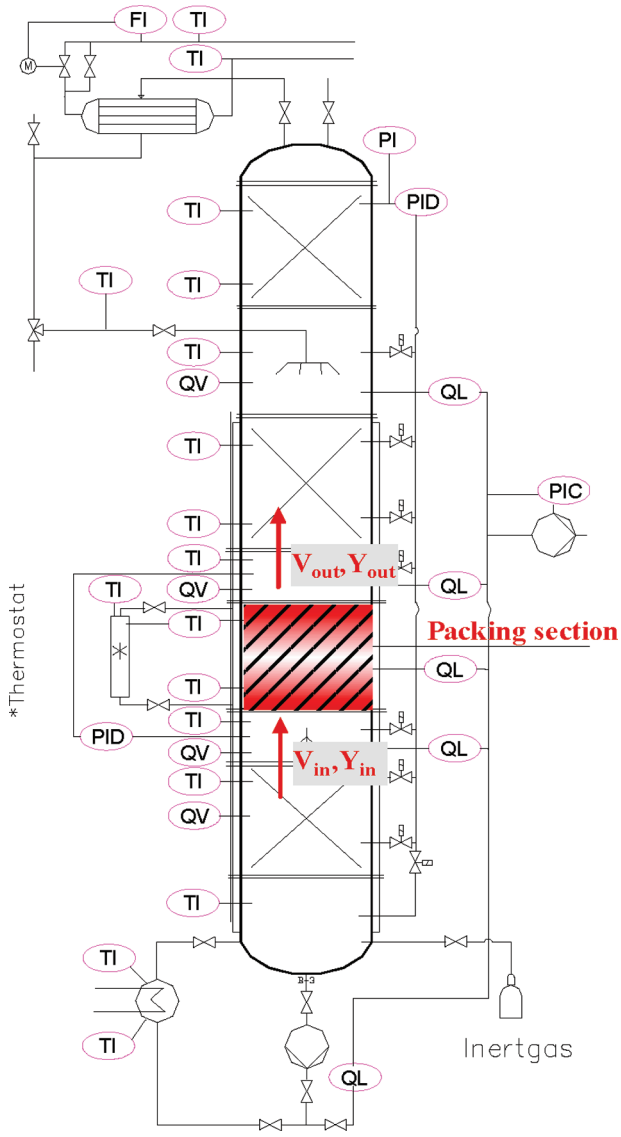

Figure 5. Process diagram of pilot plant 2 (high load conditions).

The input variables **u** contain information of packing and operation condition, i.e.,

$$\mathbf{u} = [\boldsymbol{\theta}, \Delta P, Q_{reboiler}, T_{reboiler}, \mathbf{y}_{feed}]^T \tag{44}$$

where $\boldsymbol{\theta}$ contains packing-specific parameters such as void fraction, practical area, corrugation angle, and C_P (see Table A1). The reboiler duty $Q_{reboiler}$ is given as a direct indicator of F-factor. The pressure drop ΔP, the reboiler temperature $T_{reboiler}$, and the feed composition $\mathbf{y}_{feed}$ are known as input variables too.

A number of the 55 experimental runs with three-phase packing sections are used in the flow pattern identification. The experiments cover a wide range of operation conditions (0.3−2.8 $Pa^{0.5}$). For each experiment, the flow pattern parameter η is estimated individually according to eqs 42−44, and plotted as a function of *F*-factor in Figure 6. In general, under relatively low *F*-factor (0.3−1.5 $Pa^{0.5}$) the estimated results indicate that the second liquid flows as pattern 2 (i.e., mainly above the first liquid film, $\eta \approx 0$); under relatively high *F*-factor (2.0−2.8 $Pa^{0.5}$), the second liquid is found to flow as pattern 1 (i.e., mainly below the first liquid film, $\eta \approx 1$); transition from pattern 2 to pattern 1 is observed for a medium *F*-factor (1.5−2.0 $Pa^{0.5}$).

This type of flow behavior can be appropriately described by the sigmoidal function

$$\eta = \frac{1}{1 + e^{-m(F_{factor} - n)}} \tag{45}$$

The best fitted values for coefficients [*m*,*n*] are found (Montz-Pak B1-350, [3.5,1.75]; Rombopak 9M, [10,2.1]; Super-Ring 0.3, [4.5,1.66]). As shown in Figure 6, good agreement between the experimental estimations and the sigmoidal predictions is realized, which guarantees the applicability of the sigmoidal function.

This sigmoidal shaped flow behavior of the second liquid may be closely related to the pressure drops. In Figure 7, the pressure drops in three-phase distillation using different packings are plotted. For the studied system, the transition point (i.e., coefficient *n*) in sigmoidal curves seems to correspond well with the loading point[50] in Figure 7. Moreover, the parameter *m* can be approximated as the slope at the loading point. These approximations may be helpful when specifying the flow pattern parameter η because the pressure drops can be easily determined in the experiments.

A thorough explanation to the sigmoidal shaped flow behavior is not managed at this stage. Different flow patterns of the second liquid phase have been observed in the experiments[43−45] and CFD[38,39] studies. However, the transition between the flow patterns is too complex to be predicted and the mechanism is not well understood. The explanation for this unique flow behavior may be that below the loading point, the vapor load is not strong, and there is no strong interaction between both liquids. Liquid−liquid delamination is expected and the rivulets tend to flow stably above the first liquid film since the liquid−liquid interface is free of friction and smoother than the packing surface. Above the loading point, downflow of the rivulets is greatly hindered by the vapor flow, and violent agitation between vapor phase and liquid phases may occur. In this case, the rivulets are forced by the strong vapor flow and "hide" themselves behind the first liquid film. Therefore, a transition flow from pattern 2 to pattern 1 might be reasonable when the three-phase columns are operated around the loading point. This statement can explain the observation, but a more detailed analysis is definitely needed in the future.

In this study, the sigmoidal function in eq 45 is used to calculate the flow pattern parameter η, to perform NEQ simulation and model validation.

4.3. Model Validation. The theoretical three-phase mass transfer model is validated by another 84 experimental data sets generated by plant 1 and plant 2. A comparison of experimental results (denoted as "exp") and simulated predictions (denoted as "sim") is shown in Figure 8. The vapor molar fractions of *n*-butanol and *n*-propanol are plotted and show satisfactory agreement between experiments and simulations. Almost all the data points fall within the ±10% relative error lines, which verify the reliability of the proposed mass transfer model.

In the simulations, the surface variations on the effective interfacial area $a_e^{V'}$ are available. The predicted overall surface variation factor F_{SV} is depicted in Figure 9. A reduction on $a_e^{V'}$ is revealed for the three-phase distillations performed in plant 1. For plant 2, however, both surface reduction and surface enlargement are observed. As shown in Figure 9, for the *n*-butanol/water/*n*-propanol system, the effective interfacial area $a_e^{V'}$ generally increases as the *F*-factor increases. This indicates that, if the three-phase distillation is operated under relatively high load conditions, the mass transfer and the separation efficiency would be enhanced. This information might be valuable for design and operation of a three-phase distillation process similar to the *n*-butanol/water/*n*-propanol system.

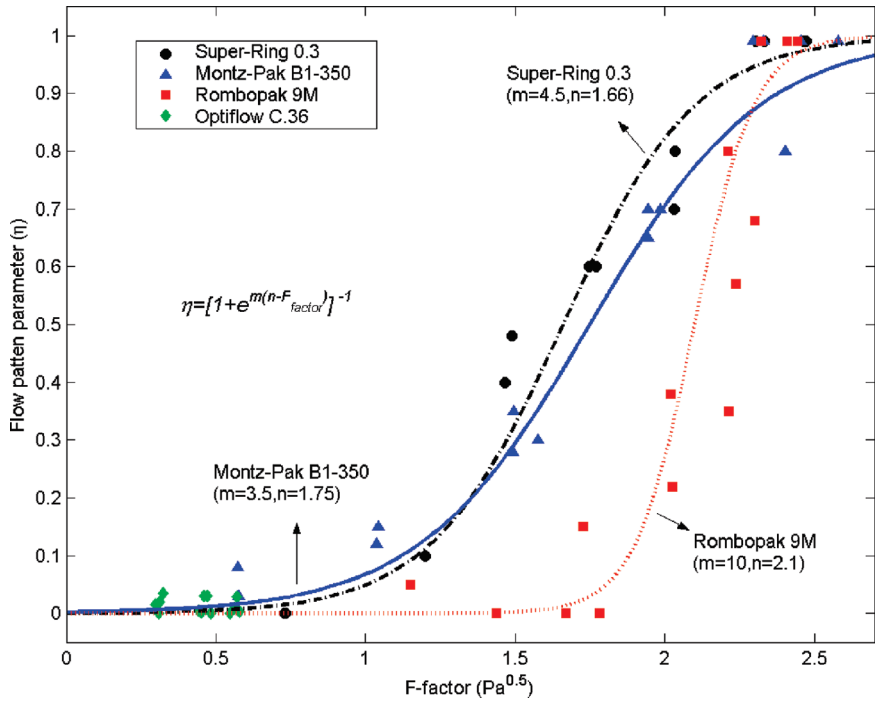

Figure 6. Flow pattern identification: a representation of sigmoidal functions for different packing under different *F*-factors.

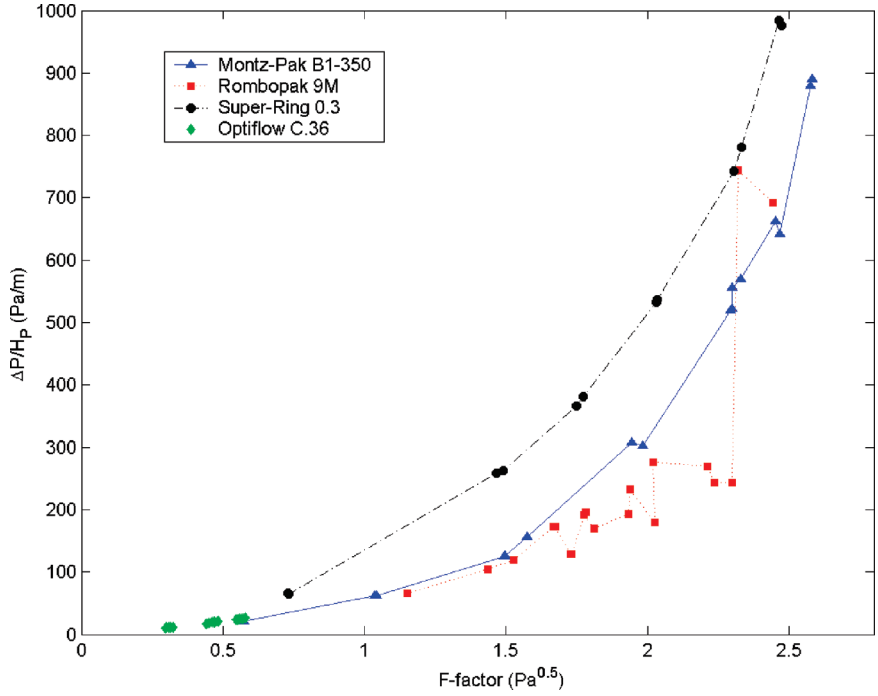

Figure 7. Experimental measurements of pressure drops for different packings as function of *F*-factor.

The variations of effective interfacial area are rooted in the changes of the second liquid phase flow pattern. When the column is operated below the loading point, the second liquid flows mainly above the first liquid film ($\eta \approx 0$), and surface reduction is therefore expected. As the load condition increases, the second liquid turns to flow below the first liquid film ($\eta \approx 1$), which results in the enlargement of the effective interfacial area. In Figure 9, a transition from reduced a_e^V to enlarged a_e^V happens near the loading points, which agrees well with those transition points observed in Figures 6 and 7.

4.4. Droplets Effect. The droplet-flow may also occur in the three-phase distillation as observed in prior experimental[43–45] and CFD[38,39] studies. The droplets are assumed to split from the rivulets as they flow down the packing element. In most cases, the droplets have small volume, and therefore were not considered in previous sections. However, under high load operations above the loading point, the violent agitation may inhibit the establishment of continuous rivulets, and the formation of the droplets on the packing element will be greatly promoted.

We assume the droplets have the same flow pattern as the rivulets. Therefore, under high load operations, they would mainly flow below the first liquid film, and enlarge the effective interfacial area a_e^V significantly. The unit surface enlargement

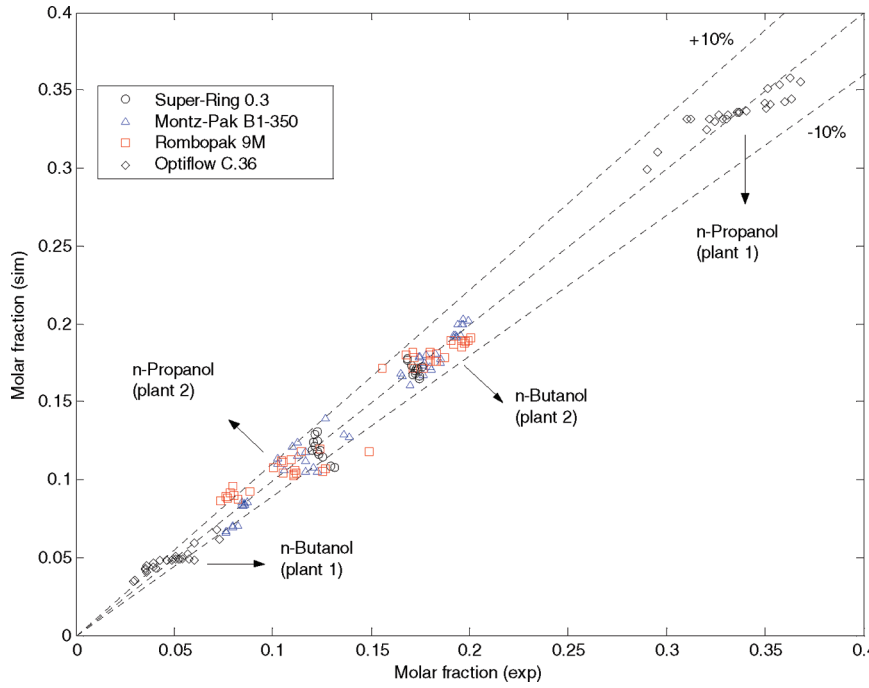

Figure 8. Model validation: a comparison of experimental and simulated results represented by vapor molar fractions.

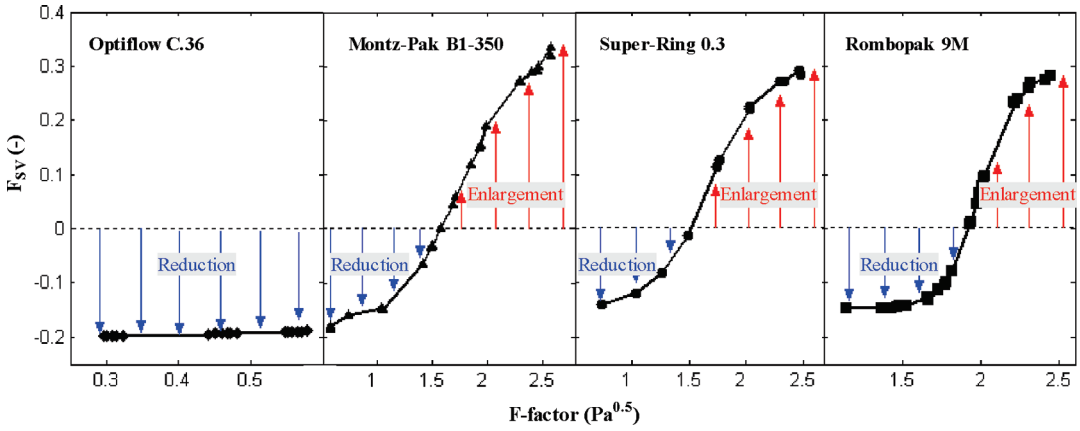

Figure 9. Variations of effective interfacial area as function of *F*-factor.

factor f^+ achieved by a single droplet is derived (in a similar deduction as for rivulet in Appendix 1)

$$f^+ = 2 \quad \text{with} \quad \phi^+_{\min} = \frac{1}{(1 + \delta_f/\delta_r)^3 - 1} \tag{46}$$

Comparing eq 46 with eq 1, it is revealed that the droplets can achieve a larger enlargement with a smaller volumetric ratio. Extending eq 6 by taking into account the droplet effect, the overall surface variation factor by droplets F^d_{SV} can be approximated as

$$F^d_{SV} = \left(1 + \frac{\delta_f}{\delta_r} + \frac{1}{2 + \dfrac{\delta_f}{\delta_r}}\right) F_{SV}, (F^d_{SV} \in [-1, 1]) \tag{47}$$

In the model validation, as shown in Figure 8, there are data points that lie outside the ±10% limitations. These data are found to be generated under high *F*-factor operations. These deviations between experiments and simulations could be attributed into the droplets effect as illustrated below.

The total mass transfer rate of *n*-propanol from the vapor phase to the first and the second liquid phases is plotted in Figure 10. The experimental results are calculated as

$$\dot{n}_3 = V_{out} y_{out,3} - V_{in} y_{in,3} \tag{48}$$

and in a three-phase NEQ model, it can be calculated as

$$\dot{n}_3 = \sum_{j=1}^{N_P} \left((N^{V'}_{j,3}) a^{V'}_j + (N^{V''}_{j,3}) a^{V''}_j \right) \tag{49}$$

The droplet formation under high load conditions is confirmed by Figure 10. The mass transfer model considering droplets effect shows better trace ability under high *F*-factor operations. The possible cause for the fast increased mass transfer rates is likely that the aqueous droplets are enveloped by the organic film under high load conditions, and increase the V−L′ interface (the main interface for mass transfer) dramatically. As given in eq 47, the overall enlargement effect achieved by droplets is larger than that achieved by rivulets.

4.5. HTU Estimation. The discrepancy on separation efficiencies of three-phase packed distillation has seldom been

successfully explained. In this section, more insights are provided to enlighten the discrepancy existing in separation efficiencies (represented by HTU value in this study).

In a ternary system, the estimated separation efficiency of component i can be calculated as

$$HTU_{i,OV} = \frac{H}{NTU_{i,OV}} = \frac{H}{\int_{y_{i,in}}^{y_{i,out}} \frac{dy_i}{y_i^* - y_i}} \tag{50}$$

Repke et al.[26] proposed a recursion procedure to calculate the equilibrium concentration y_i^*. In the experiment, when the measurements $y_{i,in}$ and $y_{i,out}$ are known, the experimental HTU_{OV} value can be calculated by eq 50.[26,33−35]

Alternatively, in the NEQ simulation of this study, a numerical integral is used with simulated concentrations.

$$NTU_{i,OV} = \int_{y_{i,in}^{sim}}^{y_{i,out}^{sim}} \frac{dy_i}{y_i^* - y_i} = \int_{y_{i,in}^{sim}}^{y_{i,1}^{sim}} \frac{dy_i}{y_{i,1}^* - y_{i,1}} + \cdots + \int_{y_{i,N_P-1}^{sim}}^{y_{i,out}^{sim}} \frac{dy_i}{y_{i,N_P-1}^* - y_{i,N_P-1}} \approx \sum_{j=1}^{N_P} NTU_{i,j,OV} \tag{51}$$

Along the limited height of one packing section, a constant $y_{i,j}^*$ is assumed. Therefore,

$$NTU_{i,j,OV} = \int_{y_{i,j-1}^{sim}}^{y_{i,j}^{sim}} \frac{dy_i}{y_{i,j-1}^* - y_{i,j-1}} = \ln |y_{i,j} - y_{i,j}^*| \Big|_{y_{i,j-1}^{sim}}^{y_{i,j}^{sim}} \tag{52}$$

In the NEQ simulation, the vapor equilibrium concentration y_i^* is replaced by the interfacial molar fraction, i.e., $y_{i,j}^* \approx y_{i,j}^{V'}$. In this study, the simulated HTU_{OV} values are predicted by eqs 51 and 52.

A comparison of simulated and experimental HTU_{OV} (represented by the component *n*-propanol) for two-phase distillation and three-phase distillation is given in Figure 11. Referring to Table 1, the discrepancy of the separation efficiency of *n*-butanol/water/*n*-propanol system could be somehow explained.

• Based on experiments carried out in plant 1, Repke et al.[26] reported a decrease in efficiency for three-phase distillation. The relevant experimental and simulated results are shown in Figure 11a. The predicted separation efficiencies show good agreement with the experimental statements.

• Villain et al.[33−35] carried out other investigations using plant 2. They mentioned a slightly increased (or unchanged) efficiency for medium F-factor (1.0−2.0 $Pa^{0.5}$) operations. For high F-factor conditions (2.0−2.8 $Pa^{0.5}$), an obvious increase is observed. These results are available in Figure 11b−d. The predicted component efficiencies (for both two-phase and three-phase distillation) show fairly good tracking ability to the experimental data over a wide range of F-factor conditions.

The change of effective interfacial area plays an essential role in the change of separation efficiency. When the second liquid phase flows above the first liquid film at low load conditions, the reduced interfacial area $a^{V'}$ responds to the decreased efficiency. When the second liquid phase flows below the first liquid film at high load conditions, the enlarged $a^{V'}$ responds to the increased efficiency. When the column is operated around the loading point, the change of interfacial area is not so obvious that unchanged efficiencies may be observed.

A recent publication[51] on a three-phase falling film absorption process reported the same conclusions, i.e., they observed increased efficiency when the rivulets and droplets flowed below the absorption falling film, and decreased efficiency when the second liquid flowed above the falling film. These results in another way confirm the reliability of the proposed mass transfer model.

When designing a three-phase distillation, it is of great importance to ensure the column is operated under suitable load conditions, e.g., the *n*-butanol/water/*n*-propanol system may be best operated above the loading point to achieve optimal separation efficiency. The proposed mass transfer model would be helpful since it provides more rigorous modeling of the intrinsic mass transfer features in a three-phase packed column.

5. Conclusion

To explore the essence of the three-phase packed column, a theoretical mass transfer model was developed and verified using the experimental facilities at the Institute of Process Engineering, TU Berlin. The mass transfer model, containing rigorous computation of all the transfer parameters (i.e., effective interfacial areas and binary mass transfer coefficients) between all V−L′, V−L″, L′−L″ interfaces, enables rate-based mass transfer calculation for NEQ simulation of three-phase packed distillation processes. For the studied *n*-butanol/water/*n*-propanol

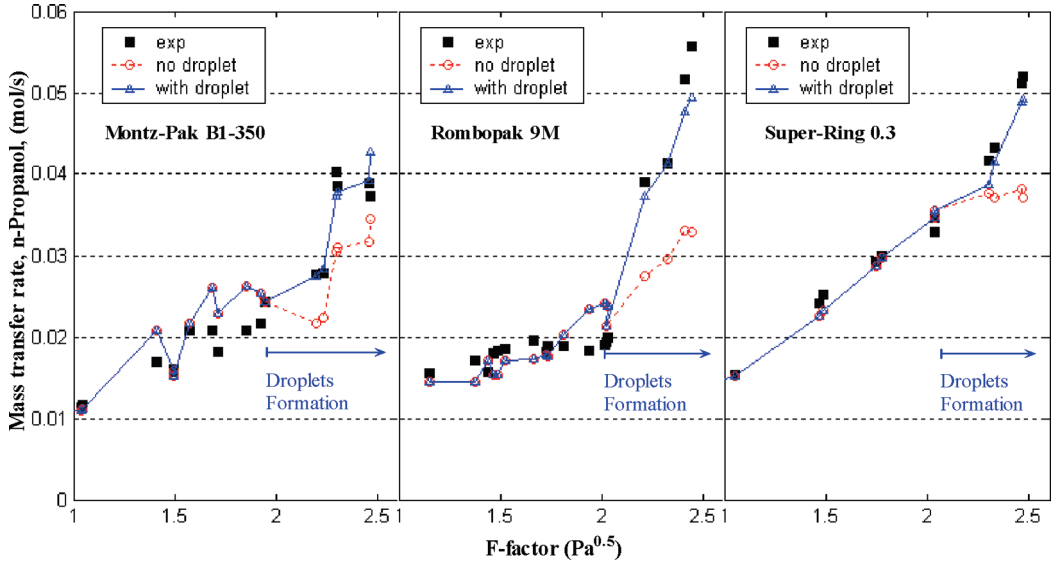

Figure 10. Evaluation of droplets effect considering droplet formation under high load conditions.

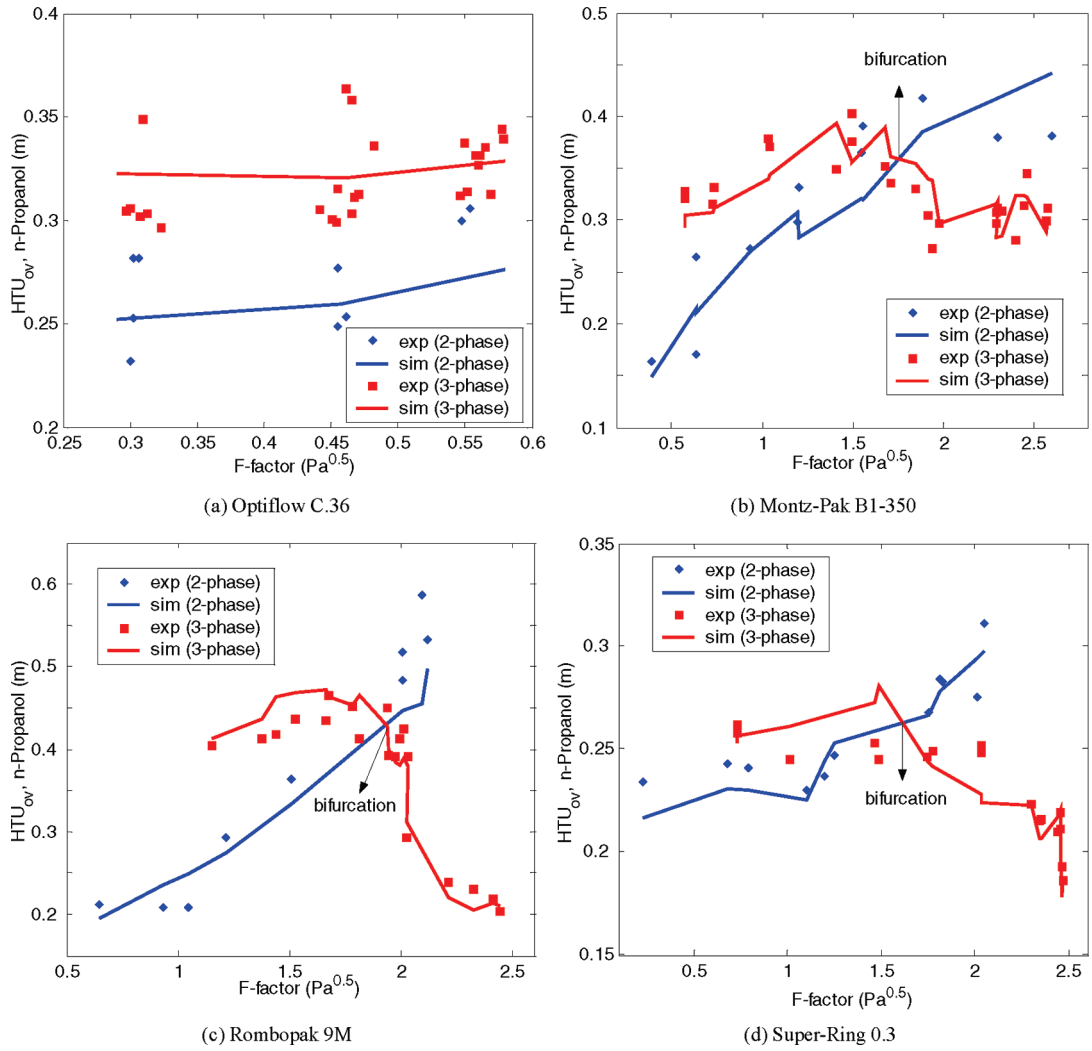

Figure 11. Comparison of experimental and simulated separation efficiencies of two-phase and three-phase distillation.

mixture, it is revealed that the second liquid phase flows mainly above the first liquid film at low load conditions, and trends to flow below the first liquid film at high load conditions. The change of the flow pattern accounts for the variation of the main mass transfer interfacial area, and will fundamentally change the separation performance in a three-phase system. This unique flow behavior may essentially result in the discrepancy of the separation efficiencies in the three-phase columns. Experimental model validation shows the validity of the proposed three-phase mass transfer model.

More experimental data on three-phase distillation will be explored further. Experiments on the mixture acetone/toluene/water[30–35] and the mixture acetone/tetrachloroethylene/water[30,33–35] exhibit concentration profiles and efficiency results similar to those in this study. These data will be adopted in future work to support and refine the mass transfer model for three-phase packed distillation.

Appendix 1

Unit Surface Enlargement and Reduction

As shown in Figure A1, surface enlargement is achieved when a single rivulet flows below the first liquid film. The unit surface enlargement factor f^+ is derived as below.

When the second liquid does not appear, the surface area is

$$S_o = l \cdot 2(\delta_r + \delta_f) \tag{A1}$$

If the rivulet appears, the enlarged surface area is

$$S_E = l \cdot \pi(\delta_r + \delta_f) \tag{A2}$$

The surface enlargement is achieved.

$$f^+ = \frac{S_E}{S_o} = \frac{\pi}{2} \tag{A3}$$

To achieve the enlargement, the volumetric ratio of the second/first liquid is at least

$$\phi^+_{\min} = \frac{\dot{V}_r}{\dot{V}_f} = \frac{l \cdot \pi/2 \cdot \delta_r^{\,2}}{l \cdot \pi/2 \cdot (\delta_r + \delta_f)^2 - l \cdot \pi/2 \cdot \delta_r^{\,2}} = \frac{1}{(1 + \delta_f/\delta_r)^2 - 1} \tag{A4}$$

As shown in Figure A2, surface area is reduced when a single rivulet flows above the first liquid film. The unit surface reduction factor f^- is calculated as below. The surface area covered by the rivulet is excluded from mass transfer. Hence,

$$f^- = 0 \tag{A5}$$

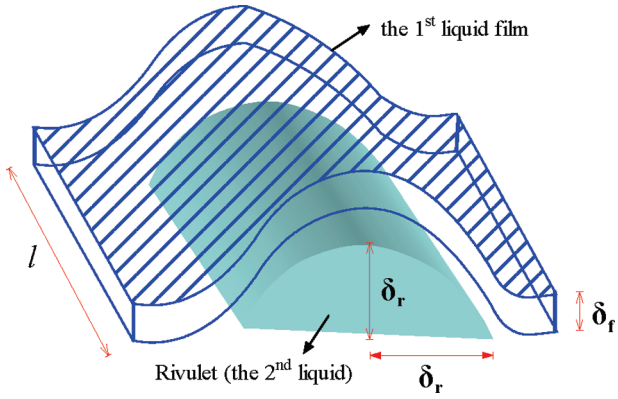

Figure A1. Surface enlargement achieved by a single rivulet flowing below the first liquid film.

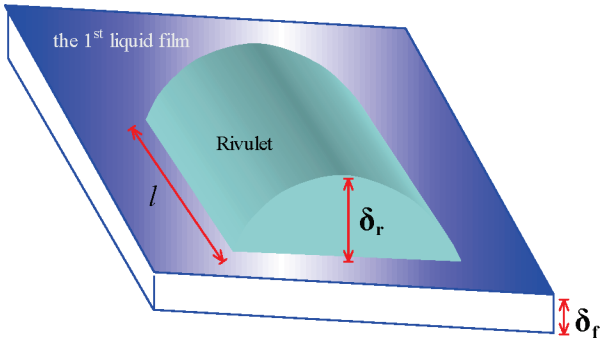

Figure A2. Surface reduction achieved by a single rivulet flowing above the first liquid film.

To achieve the reduction, the volumetric ration of the second/first liquid is at least

$$\phi_{\min}^{-} = \frac{\dot{V}_r}{\dot{V}_f} = \frac{l \cdot \pi/2 \cdot \delta_r^{\,2}}{l \cdot 2\delta_r \delta_f} = \frac{\pi \delta_r}{4\delta_f} \tag{A6}$$

Table A1. Values of Packing-Related Parameter for Effective Interfacial Area Computation

packing	C_P
Montz-Pak B1-350	0.56
Raschig Super-Ring 0.3	0.79
Rombopak 9M	0.72
Sulzer Optiflow C.36	0.51

Appendix 2

Mass Transfer Model for Two-Phase Packed Distillation

Vapor-Side Mass Transfer. The vapor-side controlled mass transfer can be described as a function of vapor phase diffusion coeffients and vapor-side Reynolds number Re_V and Schmidt number Sc_V, i.e., $\beta^V = f(D_V, Re_V, Sc_V)$.[54]

In this study, they are computed as

$$\beta^V = C_V \frac{D_V}{d_h} (Re_V)^{2/3} (Sc_V)^{1/3}, \; C_V \approx 0.12 \tag{A7}$$

Liquid-Side Mass Transfer. The liquid-side binary mass transfer coefficients are usually computed by penetration theory[21] as $\beta^L = 2[(D^L)/(\pi t_{res})]^{0.5}$, where t_{res} is the residence time for liquid flow within packing channels, i.e., $t_{res} = d_h/U_{Le}$. Hence, β^L can be computed by the relationship

$$\beta^L = C_L \sqrt{\frac{D_L U_L}{\pi d_h \varepsilon h_L \sin\theta}}, \; C_L \approx 2 \tag{A8}$$

Effective Interfacial Area. To compute the effective interfacial area a_e, the Billet and Schultes correlation[53] is modified to take into account the effect of contact angle and the influence of vapor load.

$$\frac{a_e}{a_p} = C_P (U_V \sqrt{\rho_V})^{-0.2} \varepsilon^{-0.5} (\cos\gamma)^{0.7} (Re_L)^{-0.2} (We_L)^{0.75} (Fr_L)^{-0.45} \tag{A9}$$

where

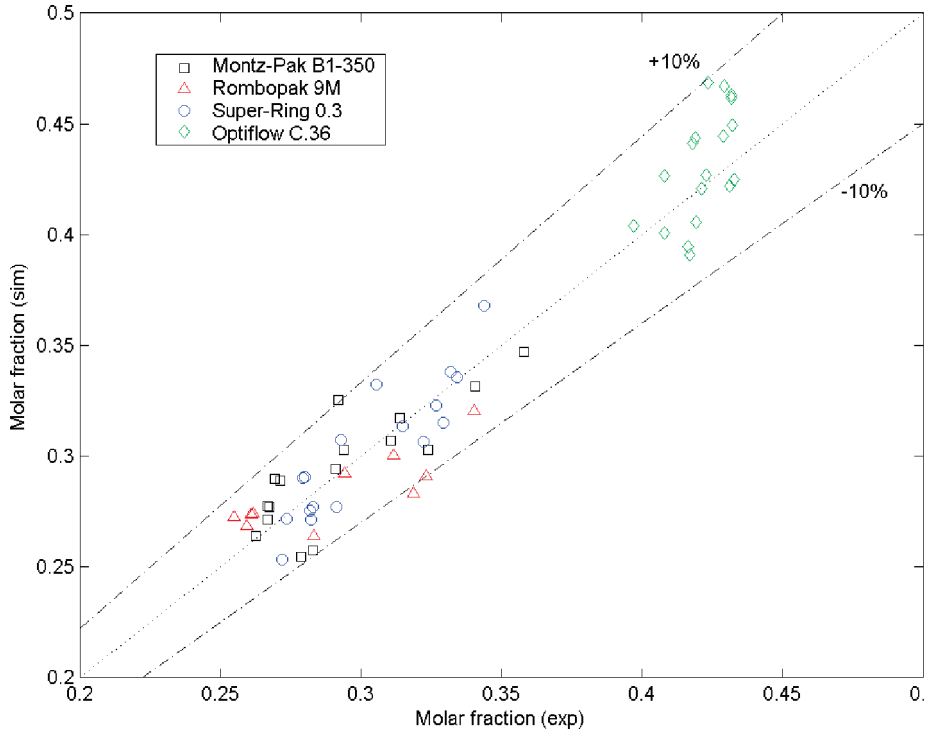

Figure A3. Experimental validation of the two-phase mass transfer model by vapor phase molar fractions of *n*-propanol.

$$Re_V = \frac{\rho_V U_{Ve} d_h}{\mu_V},\ Sc_V = \frac{\mu_V}{\rho_V D_V},\ Re_L = \frac{\rho_L U_{Le} d_h}{\mu_L},$$
$$We_L = \frac{U_{Le}^2 \rho_L d_h}{\sigma_L},\ Fr_L = \frac{U_{Le}^2}{d_h g} \quad \text{(A10)}$$

and C_P is a packing related parameter that represents the packing geometric properties. For some packings used in our experiments, these values are estimated based on the experimental data, and given in Table A1.

The above correlations built up a mass transfer model for two-phase distillation. Experimental model validation shown in Figure A3 confirms the applicability of the mass transfer model. The experimental data were generated by pilot plant 1 and plant 2.

Nomenclature

a = interfacial area [m^2]
a_e = effective interfacial area [m^2/m^3]
a_p = packing specific area [m^2/m^3]
A_c = cross section of the column [m^2]
$[B]$ = matrix of inverse mass transfer coefficient [s/m]
C_t = molar density [mol/m^3]
d_h = hydraulic diameter [m]
D = binary diffusion coefficient [m^2/s]
f = unit surface enlargement (reduction) factor [-]
F = enlargement (reduction) factor [-]
F_{SV} = overall surface variation factor [-]
Fr = Froude number [-]
$\mathbf{g}$ = equality constrains (NEQ model equations) [-]
$\mathbf{h}$ = inequality constrains [-]
h_L = liquid holdup [m]
HTU_{OV} = overall height of a transfer unit [m]
J = molar diffusion flux [mol/m^{2}s]
$[k]$ = matrix of multicomponent mass transfer coefficient [m/s]
L = liquid flow rate [mol/s]
$\dot{n}$ = mass transfer rate [mol/s]
M = molar mass [kg/kmol]
N = interfacial mass transfer flux [mol/m^2·s]
N_C = number of component in the mixture [-]
N_P = number of packing segments [-]
NTU_{OV} = overall number of transfer units [-]
Re = Reynolds number [-]
Sc = Schmidt number [-]
U = superficial velocity [m/s]
V = vapor flow rate [mol/s]
We = Weber number [-]
x = liquid molar fraction [mol/mol]
y = vapor molar fraction [mol/mol]
z = mole fraction [mol/mol]
ΔZ = height of the packing segment [m]

Greek Symbols

β = binary mass transfer coefficient [m/s]
γ = contact angle [°]
δ = film thickness [m]
ε = packing void fraction [m^3/m^3]
ρ = density [kg/m^3]
η = flow pattern parameter [-]
ϕ = volumetric ratio [-]
θ = corrugation angle [°]
$\mathbf{\Phi}$ = objective function [-]
$[\Gamma]$ = correction matrix of thermodynamic factors [-]
$[\Xi]$ = correction matrix for high flux [-]

Subscripts and Superscripts

L = liquid
V = vapor
$'$ = first liquid phase
$''$ = second liquid phase
d = droplet (second liquid)
r = rivulet (second liquid)
f = film (first liquid)
$+$ = enlargement effect
$-$ = reduction effect

Acknowledgment

L.C. thanks Technische Universität Berlin for providing him the "Sandwich scholarship" to pursue further research in Germany.

Literature Cited

(1) Lao, M.; Taylor, R. Modeling Mass Transfer in Three-Phase Distillation. *Ind. Eng. Chem. Res.* **1994**, *33*, 2637.
(2) Ottenbacher, M.; Hasse, H. Continuous Three-Phase Distillation: A Process for Separating Thermally Unstable Substances. *Chem. Eng. Res. Des.* **2007**, *85*, 144.
(3) Qi, Z.; Sundmacher, K. Bifurcation Analysis of Reactive Distillation Systems with Liquid-Phase Splitting. *Comput. Chem. Eng.* **2002**, *26*, 1459.
(4) Gumus, Z. H.; Ciric, A. R. Reactive Distillation Column Design with Vapor/Liquid/Liquid Equilibria. *Comput. Chem. Eng.* **1997**, *21*, 938.
(5) Khaledi, R.; Bishnoi, P. R. A Method for Modeling Two- and Three-Phase Reactive Distillation Columns. *Ind. Eng. Chem. Res.* **2006**, *45*, 6007.
(6) Block, U.; Hegner, B. Development and Application of a Simulation Model for Three-Phase Distillation. *AIChE J.* **1976**, *22*, 582.
(7) Ross, A. B.; Seider, W. D. Simulation of Three-Phase Distillation Towers. *Comput. Chem. Eng.* **1981**, *5*, 7.
(8) Ferraris, G. B.; Morbidelli, M. Distillation Models for Two Partially Immiscible Liquids. *AIChE J.* **1981**, *27*, 881.
(9) Ferraris, G. B. An Approximate Mathematical Model for Three-Phase Multistage Separators. *AIChE J.* **1982**, *28*, 49.
(10) Kovach, J. W.; Seider, W. D. Heterogeneous Azeotropic Distillation-Homotopy-Continuation Methods. *Comput. Chem. Eng.* **1987**, *11*, 593.
(11) Kingsley, J. P.; Lucia, A. Simulation and Optimization of Three-Phase Distillation. *Ind. Eng. Chem. Res.* **1988**, *27*, 1900.
(12) Shyamsundar, V.; Rangaiah, G. P. A Method for Simulation and Optimization of Multiphase Distillation. *Comput. Chem. Eng.* **2000**, *24*, 23.
(13) Schneider, R.; Wozny, G.; Fieg, G. Optimization of an Industrial Three Phase Distillation Column Train with Experimental Verification. *Comput. Chem. Eng.* **1997**, *21*, 1131.
(14) Widagdo, S.; Seider, W. D.; Sebastian, D. H. Bifurcation Analysis in Heterogeneous Azeotropic Distillation. *AIChE J.* **1989**, *35*, 1457.
(15) Cairns, B. P.; Furzer, I. A. Multicomponent Three-Phase Azeotropic Distillation. 3. Modern Thermodynamic Models and Multiple Solutions. *Ind. Eng. Chem. Res.* **1990**, *29*, 1383.
(16) Kovach, J. W.; Seider, W. D. Heterogeneous Azeotropic Distillation: Experimental and Simulation Results. *AIChE J.* **1987**, *33*, 1300.
(17) Herron, C. C.; Kruelskie, B. K.; Fair, J. R. Hydrodynamics and Mass Transfer on Three-Phase Distillation Trays. *AIChE J.* **1988**, *34*, 1267.
(18) Stevens, R.; Furzer, I. A. Incipient Three Phase Distillation: Experimental Tray Composition Profiles. *AIChE J.* **1989**, *35*, 1199.
(19) Cairns, B. P.; Furzer, I. A. Multicomponent Three-Phase Azeotropic Distillation. 1. Extensive Experiment Data and Simulation Results. *Ind. Eng. Chem. Res.* **1990**, *29*, 1349.
(20) Taylor, R.; Krishna, R.; Kooijman, H. Real-World Modeling of Distillation. *Chem. Eng. Progress.* **2003**, *99*, 28.
(21) Taylor, R.; Krishna, R. *Multicomponent Mass Transfer*; John Wiley & Sons: New York, 1993.
(22) Mortaheb, H. R.; Kosuge, H.; Asano, K. Hydrodynamics and Mass Transfer in Heterogeneous Distillation with Sieve Tray Column. *Chem. Eng. J.* **2002**, *88*, 59.

(23) Higler, A.; Chande, R.; Taylor, R.; Baur, R.; Krishna, R. Nonequilibrium Modeling of Three-Phase Distillation. *Comput. Chem. Eng.* **2004**, *28*, 2021.

(24) Eckert, E.; Vanek, T. Some Aspects of Rate-based Modelling and Simulation of Three-Phase Distillation Columns. *Comput. Chem. Eng.* **2001**, *25*, 603.

(25) Saito, N.; Abe, Y.; Kosuge, H.; Asano, K. Homogeneous and Heterogeneous Distillation of Ethanol-Benzene-Water System by Packed Column with Structured Packing. *J. Chem. Eng. Jpn.* **1999**, *32*, 670.

(26) Repke, J.-U.; Wozny, G. Experimental Investigations of Three-Phase Distillation in Packed Column. *Chem. Eng. Technol.* **2002**, *25*, 513.

(27) Repke, J.-U.; Wozny, G. A Short Story of Modeling and Operation of Three-Phase Distillation in Packed Columns. *Ind. Eng. Chem. Res.* **2004**, *43*, 7850.

(28) Schoenborn, E. M.; Koffolt, J. H.; Withrow, J. R. Rectification in the Presence of an Insoluble Component. *Trans. Am. Inst. Chem. Eng.* **1941**, *37*, 997.

(29) Harrison, M. E. Consider Three-Phase Distillation in Packed Columns. *Chem. Eng. Progr.* **1990**, *86*, 80.

(30) Krämer, J. Multiphase Flow and Mass Transfer in Three-Phase Packed Distillation. *Fortschritt-Berichte VDI-Z. Reihe 3*; VDI-Verlag: Duesseldorf, Germany, 1996; No. 432.

(31) Siegert, M. Three-Phase Distillation in Packed Columns. *Fortschritt-Berichte VDI-Z. Reihe 3*; VDI-Verlag: Duesseldorf, Germany, 1999; No. 586.

(32) Siegert, M.; Stichlmair, J.; Repke, J.-U.; Wozny, G. Heterogeneous Azeotropic Distillation in Packed Columns: Experimental Results. *Chem. Eng. Technol.* **2000**, *23*, 1047.

(33) Villain, O.; Repke, J.-U.; Wozny, G. Systematic Experimental Investigation of the Three-Phase Distillation. Presented at the *15th International Conference Process Engineering & Chemical Plant Design*, 2004, Krakow.

(34) Villain, O.; Repke, J.-U.; Wozny, G. Evaluation of Separation Efficiency of Three-Phase Operated Packed Towers. Presented at AIChE Spring Meeting, 2005.

(35) Villain, O.; Repke, J.-U.; Wozny, G. Performance Characterization of Three-phase Operated Column. Presented at AIChE Annual Meeting, 2003.

(36) Taylor, R. Distillation Modeling After All These Years: A Review of the State of Art. *Ind. Eng. Chem. Res.* **2007**, *46*, 4349.

(37) Springer, R.; Baur, R.; Krishna, R. Composition Trajectories for Heterogeneous Azeotropic Distillation in a Bubble-Cap Tray Column: Influence of Mass Transfer. *Chem. Eng. Res. Des.* **2003**, *81*, 614.

(38) Paschke, S.; Repke, J.-U.; Wozny, G. Untersuchungen von Filmströmungen mittels eines neuartigen Micro Particle Image Velocimetry Messverfahrens. *Chem. Ing. Technik.* **2008**, *80*, 1477.

(39) Hoffmann, A.; Ausner, I.; Repke, J.-U.; Wozny, G. Detailed Investigation of Multiphase (Gas-Liquid and Gas-Liquid-Liquid) Flow Behavior on Inclined Plates. *Chem. Eng. Res. Des.* **2006**, *84*, 147.

(40) Mahr, B.; Mewes, D. Two-Phase Flow in Structured Packings: Modeling and Calculation on a Macroscopic Scale. *AIChE J.* **2008**, *54*, 614.

(41) Egorov, Y.; Menter, F.; Klöker, M.; Kenig, E. Y. On the Combination of CFD and Rate-based Modelling in the Simulation of Reactive Separation Processes. *Chem. Eng. Process.* **2005**, *44*, 631.

(42) Ataki, A.; Bart, H.-J. Experimental and CFD Simulation Study for the Wetting of a Structured Packing Element with Liquids. *Chem. Eng. Technol.* **2006**, *29*, 336.

(43) Hoffmann, A.; Ausner, I.; Repke, J.-U.; Wozny, G. Fluid Dynamics in Multiphase Distillation Processes in Packed Towers. *Comput. Chem. Eng.* **2005**, *29*, 1433.

(44) Repke, J.-U.; Ausner, I.; Paschke, S.; Hoffmann, A.; Wozny, G. On the Track to Understanding Three Phases in One Tower. *Chem. Eng. Res. Des.* **2007**, *85*, 50.

(45) Xu, Y.; Paschke, S.; Repke, J.-U.; Yuan, J.; Wozny, G. Portraying the Countercurrent Flow on Packings by Three-Dimensional Computational Fluid Dynamics Simulations. *Chem. Eng. Technol.* **2008**, *31*, 1445.

(46) Guo, M. Q.; Wang, S. Q.; Repke, J.-U.; Wozny, G. Nonequilibrium Model and Parameter Estimation on Three-Phase Distillation in a Packed Column. Presented at the *5th World Congress on Intelligent Control and Automation (WCICA)*, 2004, Hangzhou, China.

(47) Krishnamurthy, R.; Taylor, R. A. Nonequilibrium Stage Model of Multicomponent Separation Processes. l. Model Description and Method of Solution. *AIChE J.* **1985**, *31*, 449.

(48) Krishna, R.; Standart, G. L. A Multicomponent Film Model Incorporating a General Matrix Method of Solution to the Maxwell-Stefan Equations. *AIChE J.* **1976**, *22*, 383.

(49) Joeng, S.; Garimella, S. Falling-Film and Droplet Mode Heat and Mass Transfer in a Horizontal Tube LiBr/Water Absorber. *Int. J. HeatMass Transfer* **2002**, *45*, 1445.

(50) Verschoof, H.-J.; Olujic, Z.; Fair, J. R. A General Correlation for Predicting the Loading Point of Corrugated Sheet Structured Packings. *Ind. Eng. Chem. Res.* **1999**, *38*, 3663.

(51) Paschke, S.; Thiele, R.; Repke, J.-U. Untersuchung des Stoffübergangverhaltens Dreiphasig Betriebener Fallfilmabsorber. *Chem. Ing. Technik.* **2009**, *81*, 297.

(52) Nicolaiewsky, E. M. A.; Tavares, F. W.; Rajagopal, K.; Fair, J. R. Liquid Film Flow and Area Generation in Structured Packed Columns. *Power Technol.* **1999**, *104*, 84.

(53) Billet, R.; Schultes, M. Prediction of Mass Transfer Columns with Dumped and Arranged Packings: Updated Summary of the Calculation Method of Billet & Schultes. *Chem. Eng. Res. Des.* **1999**, *77*, 498.

(54) Wang, G. Q.; Yuan, X. G.; Yu, K. T. Review Mass Transfer Correlations for Packed Column. *Ind. Eng. Chem. Res.* **2005**, *44*, 8715.

(55) Chen, L.; Repke, J.-U.; Wozny, G.; Wang, S. Q. Extension of Mass Transfer Calculation for Three-Phase Distillation in Packed Column: A Nonequilibrium Model based Parameter Estimation. *Ind. Eng. Chem. Res.* **2009**, *48*, 7289.

(56) Ausner, I. Experimental Investigations on Multi-Phase Film Flows. PhD Thesis, 2006, Technische Universität Berlin.

(57) Rocha, J. A.; Bravo, J. L.; Fair, J. R. Distillation Columns Containing Structured Packings: A Comprehensive Model for Their Performance. 2. Mass-Transfer Model. *Ind. Eng. Chem. Res.* **1996**, *35*, 1660.

(58) Repke, J.-U.; Villain, O.; Wozny, G. A Nonequilibrium Model for Three-Phase Distillation in a Packed Column: Modelling and Experiments. *Comput. Chem. Eng.* **2004**, *28*, 775.

Received for review July 2, 2009
Revised manuscript received October 13, 2009
Accepted November 10, 2009

IE9010645